Mobile Robot Localization based on Ultra-Wide-Band Ranging: A Particle Filter Approach

J. González, J.L. Blanco, C. Galindo, A. Ortiz-de-Galisteo,
J.A. Fernández-Madrigal, F.A. Moreno, and J.L. Martínez *

{jgonzalez,jlblanco,cipriano,jafma,jlmartinez}@ctima.uma.es
{aortiz,famoreno}@isa.uma.es
Department of System Engineering and Automation
ETSII Campus de Teatinos, University of Málaga.
E-29071, Málaga, Spain

Abstract

This article addresses the problem of mobile robot localization using Ultra-Wide-Band (UWB) range measurements. UWB is a radio technology widely used for communications that recently is receiving increasing attention also for positioning applications. In these cases, the position of a mobile transceiver is determined from the distances to a set of fixed, well-localized beacons. Though this is a well-known problem in the scientific literature (the trilateration problem), the peculiarities of UWB range measurements (basically, distance errors and multipath effects) demand a different treatment to other similar solutions as for example those based on laser. This work presents a thorough experimental characterization of UWB ranges within a variety of environments and situations. From these experiments we derive a probabilistic model which is then used by a particle filter to combine different readings from UWB beacons as well as the vehicle odometry. To account for the possible offset error due to multipath effects, the state tracked by the particle filter includes the offset of each beacon in addition to the planar robot pose (x, y, ϕ), both estimated sequentially. We show navigation results for a robot moving in indoor scenarios covered by three UWB beacons that validate our proposal.

Key words: Mobile robot localization, Sensor characterization, Particle filter, Ultra-Wide-Band

1. Introduction

In indoor environments, a mobile robot needs to localize itself accurately because of the limited workspace. For this purpose, artificial landmarks can be placed at known locations and measurements of angular or range data to these targets can be provided by on-board laser, vision, ultrasonic, or radio sensors. Laser sensors for automated guided vehicles are commonly used in warehouses with reflectors mounted on the walls [31]. They can achieve centimeter accuracy, but they require line of sight, which can be blocked by dynamic obstacles. Cameras can also be used to detect special landmarks, such as infrared targets attached to the ceiling [32]. In this case, it is necessary to deploy a great number of landmarks since visual recognition only works for distances of a few meters. Moreover, ultrasonic sensors have been applied as artificial landmarks by measuring the time of flight of sound pulses [34]. However, ultrasonic receivers and transmitters require an additional radio link for synchronization. In the last years, the wireless communication infrastructure of offices has been also employed for

* Corresponding author: J.L. Blanco

positioning purposes. The received signal strength of the radio signal transmitted by nodes of the Ethernet [24] or the ZigBee [4] networks is used. Nevertheless, they can only provide accuracy above meter at best.

Ultra-Wide-Band (UWB) radio technology, which has been mainly used for communication [5], is recently being also considered as a promising solution for vehicle positioning. In particular, its capability for data transmission, range accurate estimation and material penetration make this technology suitable for indoor robotic applications. A typical setup for UWB-based positioning consists of a number of fixed transceivers, or *beacons*, placed at known locations in the environment and a mobile transceiver on-board the vehicle. Assuming that the known beacon positions are error-free, the position of a mobile robot can be estimated by triangulation with an accuracy only related to that of the range measurements. This approach for positioning solves the global localization problem, which refers to the localization of the robot without considering any prior information about its previous positions and movements in the environment. Regardless the number of measurements available for triangulation, using only range information will not provide any clue about the orientation of the robot which is an essential requirement for most applications. Two possible solutions exist for overcoming this limitation: a) to place two receivers on-board the robot separated as far as possible or, b) to use complementary proprioceptive sensors such as encoders, gyros, accelerometers, etc., which give us information about the vehicle motion. In this paper we have adopted this second alternative by combining UWB range data and odometry readings. This approach, quite common in mobile robotics, also presents the important advantages of providing robustness to the positioning system and of enabling the track of the vehicle pose (position and orientation) between triangulation instants, typically with a higher period than odometry readings.

A suitable approach for coping with such a sensor fusion is a probabilistic Bayesian inference framework. A well-known and widely-used method within this framework is Kalman Filtering (KF), which relies on two strong assumptions: on the one hand, both the robot motion and the observation models are linear, and on the other hand, their errors and the initial estimated probability distributions are Gaussians [22]. The first assumption is, to a certain extent, relaxed in variants such as the Extended Kalman Filter (EKF) [20] or the Unscented Kalman Filter (UKF) [21], though they still maintain the assumption that the errors in the two models are Gaussian. This requirement becomes a serious drawback when considering range-only observations, like in UWB technology: not only the sensor model is non-linear, but multi-modal distributions may be present in a variety of situations. In Figure 1 we illustrate this fact in 2D with two beacons where we usually find two peaks at the intersections of the two rings, thus giving a bimodal distribution that cannot be properly modeled as a Gaussian.

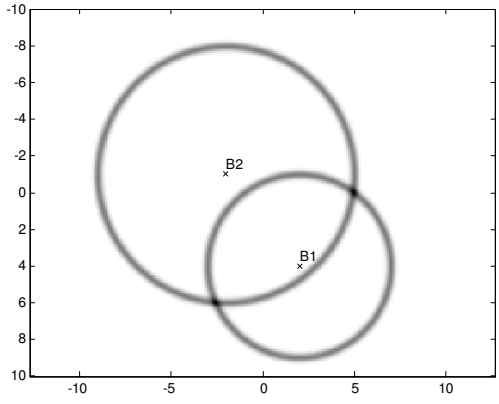

Fig. 1. Probabilistic observation likelihood for UWB range measurements in 2D for two beacons. Observe the circular Gaussian-shaped ring around each beacon. The estimated position of the vehicle is within the two intersected regions (a multi-modal distribution). Notice that, in general, the problem will be stated in 3D, using spheres instead of circles.

In this paper we address UWB-based positioning through a Monte-Carlo Bayesian filter, also known as Particle Filter (PF). PFs overcome the commented limitations by representing the estimated pose of the robot as a set of samples rather than any parametric density. Therefore, a PF can cope with non-linear models and with complex, and even multimodal distributions.

In recent literature, some works have addressed vehicle positioning based on UWB. In [23] the authors propose an algorithm for locating UWB transmitters by using a multiple-antenna array. In [27] a UWB-based communication system with localization and tracking capabilities for outdoor applications is presented. They use a set of fixed nodes to estimate the position of a set of wearable UWB devices within a controlled environment. In [13] a sled is driven through an industrial-like environment in both Line-of-Sight (LOS) and Non-Line-of-Sight (NLOS) situations while estimating its posi-

tion through UWB range measurements. A low-cost UWB local positioning system based on a Time-Difference-Of-Arrival is presented in [30] . A work closer to ours is [19], which describes a localization system combining UWB range measurements and inertial information into a particle filtering framework.

The work presented in this paper extends previous works in these two main points:

(i) We provide a comprehensive probabilistic characterization of UWB range measurements experimentally obtained for different conditions and scenarios. A variety of experiments have been conducted to derive a probabilistic model of the UWB range measurements provided by the PulsOn Kit commercialized by TimeDomain [6]. In spite of the theoretical high penetrability of the UWB signal, in the experiments in cluttered scenarios we have observed inaccuracies, spurious measurements, and the effects of multipath (multiple echoes of the transmitted signals when bounding off obstacles). This behavior makes strongly recommendable the utilization of probabilistic approaches.

(ii) We integrate such a probabilistic characterization within a PF framework for robust vehicle localization. While in most PF-based robot localization approaches the system state comprises only the position and orientation of the robot [33], in this paper we follow [19] to augment the system state in order to cope with signal multipath and spurious range measurements provided by the UWB beacons. This augmented state particle filter (ASPF) provides a plus of robustness and an improved performance in comparison to conventional approaches as demonstrated in our experiments. In comparison to [19], we provide more extensive characterization of the algorithm for a range of parameters and with three real beacons. Furthermore, in our formulation we introduce a correction of UWB systematic bias directly into the observation model.

The rest of the paper is organized as follows. The next section presents an experimental characterization of the particular UWB devices used in our work and proposes a probabilistic model to capture their behavior under different conditions. In section 3, a particle filter approach that copes with the combination of UWB range measurements and odometry is described. Results of its performance are described for two representative scenarios in section 4. Finally, some conclusions and future works are outlined.

2. Characterization of UWB Range Measurements

This section firstly gives an overview of the main characteristics of the UWB technology. Then, sections 2.2-2.3 describe a series of experiments aimed to characterize UWB range data in LOS and NLOS configurations, respectively, capturing its performance when varying the scenario and the relative position of the UWB transceivers.

2.1. *UWB Overview*

UWB is a wireless technology used in the last decades to transmit digital data for military purposes, and more recently also used for civil communications [5]. In contrast to traditional radio techniques based on sinusoidal carriers, UWB works by transmitting a radio signal over a wide swath of frequencies (in the band between 3.1 and 10.6 GHz), by means of short pulses. Since the duration of pulses is in the order of nanoseconds and they are usually spread over a wide spectrum, the energy of each transmitted pulse is very low (typically a power spectral density of -41.5 dBm/MHz). Hence, UWB can be considered as a safe system for wireless transmission and can coexist, theoretically without interference, with other radio communication technologies. Two main advantages for localization are derived from these characteristics [11,18,19,36]:

– Accurate positioning: Due to the short duration of the transmitted pulses, UWB technology offers inexpensive and accurate positioning with a resolution of centimeters. There are several methods to, theoretically, estimate the position of a moving transceiver based, for instance, on the Time of Arrival, Direction-Of-Arrival, Signal-Strength, etc. (see [16]).
– Materials penetration: The characteristics of the UWB signal transmission provide this technology with a high material penetrability, making it suitable for indoor applications. Theoretically, UWB is not affected by multipath problems [12,36], although in practice it is not completely free from that problem, as analyzed further on.

In spite of the remarkable features of UWB, it exhibits some drawbacks when used for vehicle localization in indoor, cluttered environments. Among

Fig. 2. A PulsOn transceiver. Four of these devices have been employed for the experiments described in this article.

Fig. 3. Scenario considered for UWB range characterization in LOS. Experiments have been conducted in this 3 meters-wide corridor, varying the distances between antennas from 1 to 10 m.

them is the unpredictable behavior of the transmitted signal when passing through different materials. Although UWB signals have a good penetrability they weaken when traversing obstacles, thus in practice they are prone to multipath effects which make the problem of range estimation complex and inaccurate.

In the following sections we characterize UWB ranging under two situations: (i) LOS, that is, when no obstacle obstructs the line of sight between emitter and receiver, and (ii) NLOS, when a non-penetrable obstacle (e.g., a metal panel) is between the antennas. We study in both situations the effect of varying the distance between the antennas in different types of scenarios (corridors, open areas, cluttered rooms, etc.).

It is important to remark that we do not cope here with either the physics of the UWB signal or the channel characterization. We are interested only in a probabilistic characterization of the errors of UWB-range measurements under different conditions. Although several works addressing the physics of UWB can be found in the literature (see for example [1,14,15,17,35]), the probabilistic characterization of the range measurements is a less explored topic ([2,8]).

Further sections are devoted to the experimental analysis of the range measurements provided by PulsOn kits, commercialized by TimeDomain [6] (see Figure 2).

2.2. *Characterization of UWB ranges in LOS*

The experiments described in this section aim to characterize UWB range errors in LOS when varying both the distance between the devices and the characteristics of the environment.

A first experiment was conducted in a corridor varying the distance between transceivers from 1 to 10m in steps of 1m (manually measured using a laser ranger). The experimental setup is pictured in Figure 3. At each step we have computed the systematic error, or *bias*, as the difference between the average of 5000 measured ranges from the PulsOn devices and the true distance, measured with a laser ranger. From the resulting average biases, plotted in Figure 4(a), we have observed that an exponential function fits well the evolution of the bias, thus we will adopt such function to model the UWB bias in our sensor.

To illustrate the evolution of the standard deviation of the ranges w.r.t. distance, Figure 4(c) shows some of the range histograms, their estimated means, standard deviations and respective fitted Gaussians. It is remarkable that the standard deviation is practically constant over all the distances – the differences are under 5mm, as summarized in Figure 4(b).

To sum up, from our observations we can model UWB ranges probabilistically as comprised of the following parts:

$$d_{uwb} = d_{true} + f(d) + n, \quad n \sim N(0, \sigma^2) \tag{1}$$

where d_{uwb} is the distance given by the UWB de-

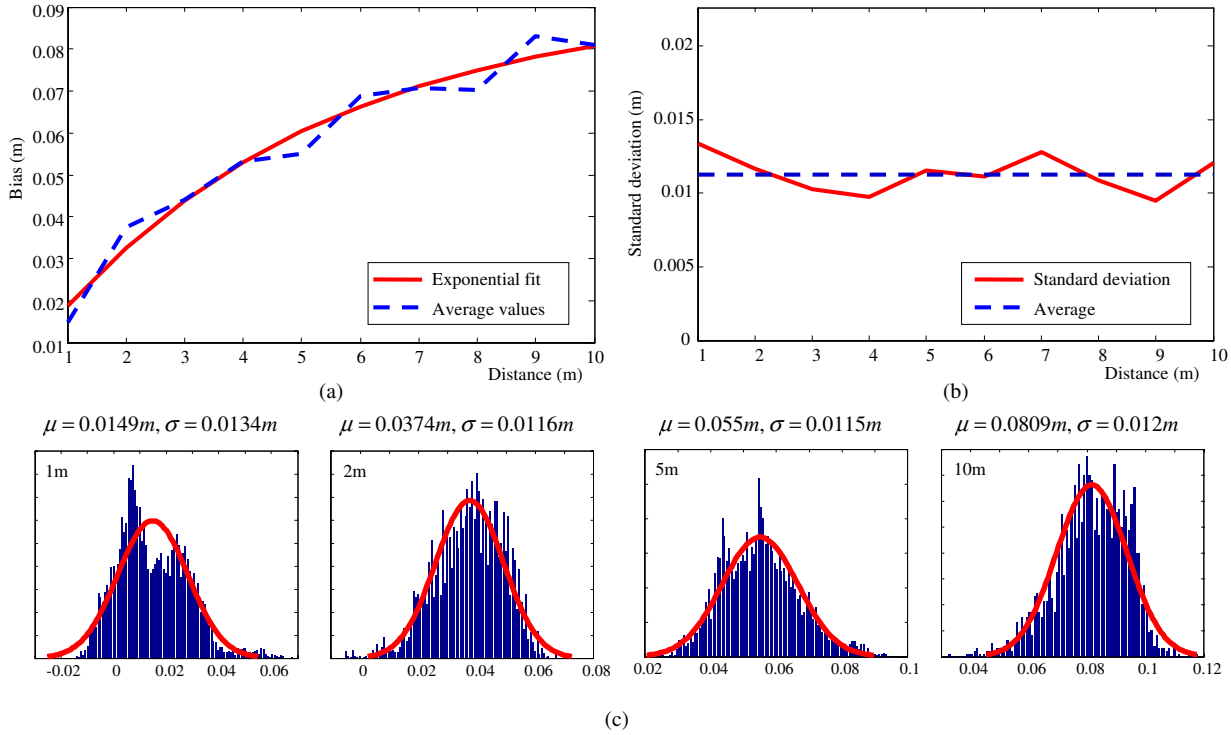

Fig. 4. UWB range characterization in a LOS configuration. (a) Evolution of the bias with the distance between the devices. Both the average of real ranges and the exponential fit are represented. (b) The corresponding standard deviations for each distance, which fall within the narrow range [0.0095,0.0134], being 0.0039m their maximum difference. (c) Histograms of the raw ranges measured at 1,2,5 and 10 metres, respectively, with Gaussian fittings. These symmetrical fittings are appropriate due to the lack of significant tails.

vice, $f(d)$ models the distance-variable systematic error (bias), and n is the random noise associated to the measurement, modeled as a zero-mean Gaussian with variance σ^2. Below we provide numerical values for these parameters. It is important to first remark that, in spite of considering a LOS configuration, multipath effects may be present due to the particular characteristics of the UWB technology and the properties of each environment: UWB signals spread in all directions, reflecting in impenetrable materials (like metal or ceramic tiles) and weakening when passing through others like walls or doors, thus constructive interferences may cause errors when calculating the time of flight. Therefore, there is not absolute confidence in a measured range to come from the direct path between the antennas.

Obviously, different multipath effects may appear in each scenario. To properly capture these effects, we have repeated the previous range characterization in other four environments: a narrower corridor, an open area, a cluttered room and an empty room. Some resulting range histograms appear in Figure 5. Since we aim to a model applicable to any environment, significant results are obtained by the combination, from all the scenarios, of histograms for each distance. Some of these final histograms appear at the right-hand side of the figure.

By computing the average bias and standard deviations, plotted in Figures 6(a)–(b) respectively, we finally come to an overall standard deviation value of $\sigma = 0.0119m$ and an exponential fit of the bias described by:

$$f(d) = 0.1\left(1.01 - e^{-0.17d}\right) \tag{2}$$

which is also represented in Figure 6(a) among the individual values used to derive this fit. Observe as well in Figure 6(b) how our assumption of a constant standard deviation fits well with the actual measurements.

2.3. *Characterization of UWB range in NLOS*

In this section we study the multipath effects in UWB ranges. To assure that the measured ranges

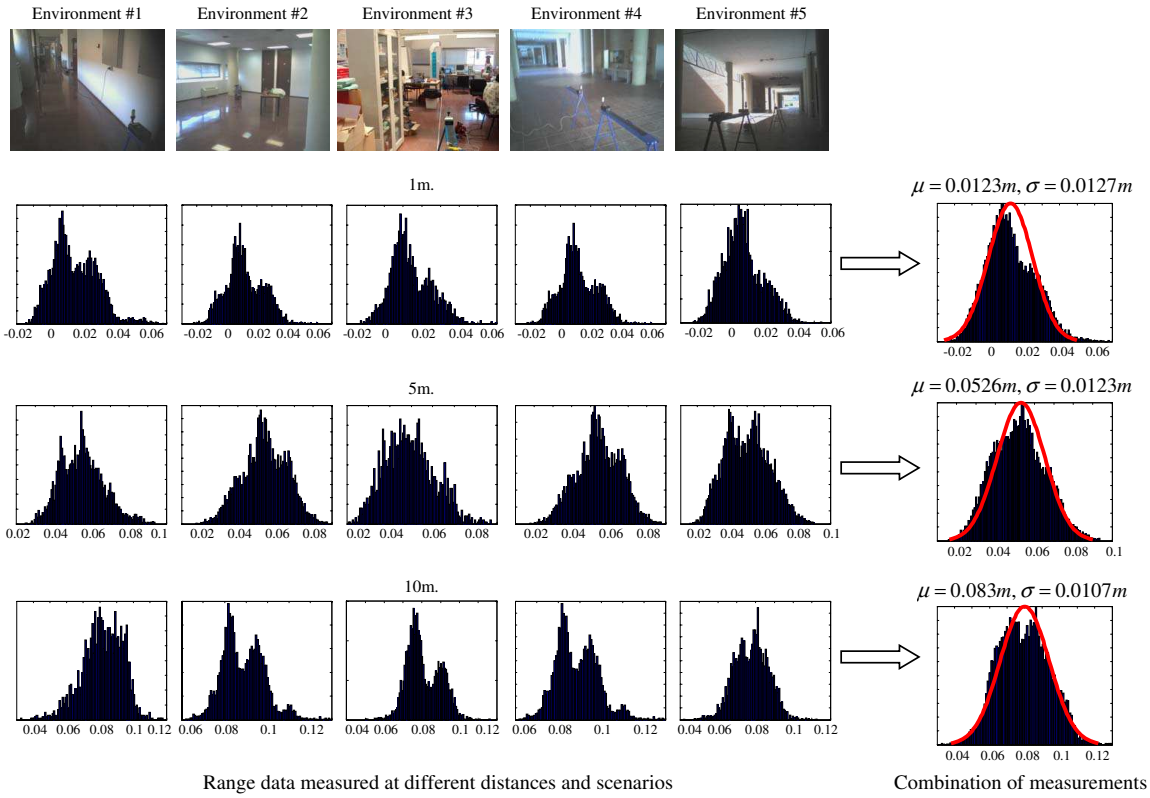

Fig. 5. LOS range characterization in five different environments. The histograms obtained for each scenario (only shown here those for 1, 5, and 10 meters of distance between antennas) are combined in order to characterize the *average* bias.

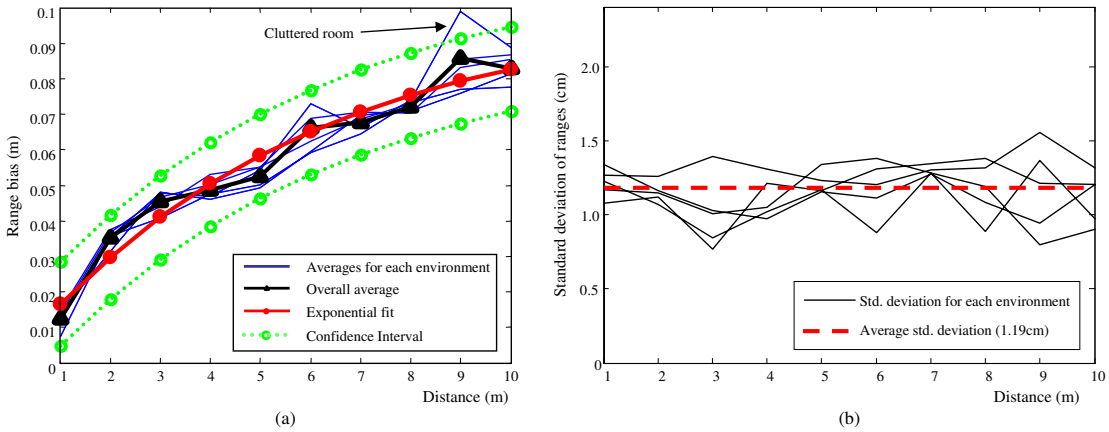

Fig. 6. (a) Range measurements in the five different environments of Figure 5, with their average, an exponential function fitting and the resulting confidence interval. Note how the cluttered scenario is the most prone to multipath and thus, the resultant bias is higher. Observe how the average bias is approximated well by the fitting function $f(d)$. (b) Evolution of the computed standard deviation for the different environments. There is no evident relation either with the antennas distance, as commented in previous experiments, nor with the specifically chosen environment.

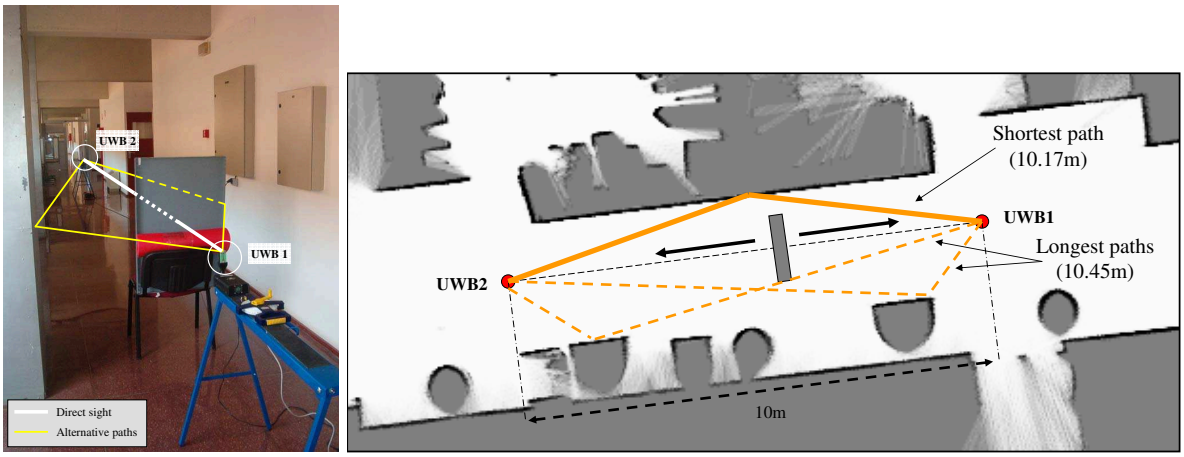

Fig. 7. Set-up considered for measuring UWB ranges under multipath effects. The shortest and longest reflections of the signals within this environment have been calculated geometrically, obtaining $10.17m$ and $10.45m$, respectively.

are affected by multipath, we set up the configuration shown in Figure 7 where, in a narrow corridor, a metal panel was placed between two UWB antennas separated 10m. The dimensions of the panel were carefully chosen to ensure that signals had to reflect on the walls before arriving at the receiver. In this scenario the shortest non-direct path between the antennas was geometrically calculated, giving 10.17m, while the longest one, considering only one reflection on the wall, was 10.45m. It is reasonable to assume that having more than one reflection weakens the energy signal too much to be detected as the main correlated pattern [6], so we can discard the possibility of having multipath caused by more than one bounce.

Figure 8(a) depicts the measured ranges when

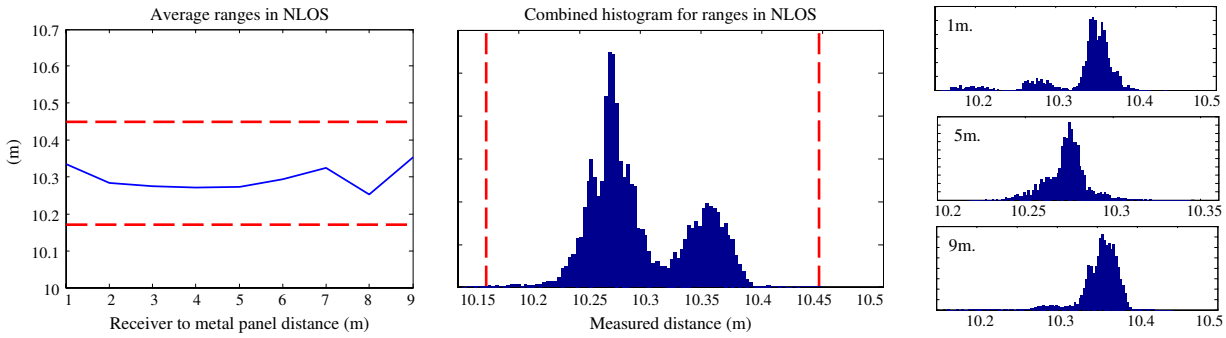

Fig. 8. Characterization of UWB ranges affected by NLOS: a metallic plane blocks the direct sight between two antennas, 10m apart from each other. Note that the average ranges in the experiment are in the interval $[10.17, 10.45]$. The multimodal histograms indicate the presence of different paths, especially for the cases in which the panel is close to one of the antennas (1m and 9 m.).

$$p(s_t|u_{1:t}, z_{1:t}) \propto p(z_t|s_t, u_{1:t}, z_{1:t-1})\, p(s_t|u_{1:t}, z_{1:t-1}) \tag{3}$$
$$= \underbrace{p(z_t|s_t)}_{\text{Observation model}} \int \underbrace{p(s_t|s_{t-1}, u_t)}_{\text{Transition model}} p(s_{t-1}|u_{1:t-1}, z_{1:t-1})\, ds_{t-1}$$

moving the metal panel between the antennas, what forces reflections to occur at different locations. As expected, the measured ranges fall within the interval $[10.17, 10.45]$. The histograms for some selected distances, shown in Figure 8(c), illustrate that there exists a more likely path followed by the signal in each case, revealed by a clear peak, but others are also possible, and thus, the measurements may be distributed over the whole interval.

The histogram in Figure 8(b) combines the recorded range distances for all the positions of the metal panel between the antennas. Notice that in a real situation there is no available information about the location of obstacles and thus, about the most probable path followed by the signals.

Therefore, the model proposed in Eq. (1) is not able to account for the random nature of multipath in NLOS configurations. Our solution to cope with multipath hence consists of extending the state vector of our particle filter in order to infer from observations how likely is that multipath exists for each particular beacon. Next section is devoted to a detailed description of this model.

3. Localization through Particle Filtering

3.1. *Problem Statement*

Methods for sequential Bayesian filtering provide a grounded probabilistic framework for tracking the state of a system which is observable only through indirect and noisy measurements. These techniques maintain a probability distribution that captures the knowledge about the state of the system at a given instant of time. This distribution changes over time following the transition model of the system and is updated with each observation by means of a probabilistic sensor model. While filters in closed form exist for Gaussian distributions and systems without nonlinearities ([20,22]), we employ here a particle filter (PF) ([9,28]) due to some important advantages within the scope of the present problem. Firstly, a PF can cope with arbitrary distributions, which enables performing global localization of the vehicle at start-up or maintaining multi-modal distributions to deal with ambiguities. Secondly, the probabilistic observation model of UWB sensors is strongly nonlinear and leads to distributions that could be hardly approximated by using Gaussians only.

We derive next the equations of our PF for robust UWB localization. Our purpose is to localize the robot within a planar environment provided a set of N beacons which have known 3D positions $\{B^k\}_{k=1}^N$. Let s_t, u_t, and z_t denote the system state, the robot actions, and the observations for any given time step t, respectively. Although we are interested in the robot pose (which we will denote as x_t), the system state also contains a set of random distance offsets $\{b_t^k\}_{k=1}^N$ from the mobile UWB transceiver to each beacon, which model the effects of multipath in NLOS conditions as discussed in section 2.3. That is, the state of the filter s_t is:

$$s_t = \left\{x_t, b_t^1, ..., b_t^N\right\} \tag{4}$$

As discussed elsewhere [19], the inclusion of these offsets into the system model provides a great improvement in terms of robustness against the effects of multipath for this kind of radio technology. Now, by assuming that the system state s_t evolves as a Markov chain, we can write down our estimation problem into the well-known sequential form in Eq. (3). To implement this recursive equation as a PF we start with a set of M samples in the state space $\{s_{t-1}^{[i]}\}_{i=1}^M$, called *particles*, which are approximately distributed according to the distribution for the previous time step $t-1$ (a uniform distribution can be assumed initially if there is no information about the robot pose). According to *importance sampling* [9], a weight $\omega_{t-1}^{[i]}$ is also associated to each particle to compensate potential mismatches between the density of samples at a given area of the state space and the actual (unknown) density. Following the most common algorithm for particle filtering, *Sequential Importance Sampling with Resampling* (SIR) [29], the set of particles for the next time step t is generated by means of the following steps:

- Generate the new particles by drawing samples from a certain proposal distribution, $q(s_t|s_{t-1}, u_t, z_t)$.
- Update the weight $\omega_{t-1}^{[i]}$ for all the new samples based on the value of the observation likelihood of each particle.
- Perform a resampling step in order to prevent the loss of particle diversity if a measure of quality of the particles, the effective sample size [25], falls below a given limit.

One of the most popular choices for the proposal distribution is the system transition model, that is, $q(s_t|s_{t-1}, u_t, z_t) = p(s_t|s_{t-1}, u_t)$. In this case, updating the importance weights becomes:

$$\omega_t^{[i]} \propto \omega_{t-1}^{[i]} p\left(z_t|\, s_t^{[i]}\right) \tag{5}$$

that is, scaling the previous weights by the observation likelihood evaluated at each particle $s_t^{[i]}$. In the next subsection we discuss in detail how to compute this term, which is in charge of fusing the sensory data from the different UWB beacons.

Regarding the system transition model, there are two separate processes involved, one for each part of the augmented state vector s_t: the robot pose and the beacon offsets. We examine them separately.

For the common case that the robot actions u_t are given by incremental odometry readings, the predicted robot pose x_t is obtained by adding the odometry to the previous pose x_{t-1} and by corrupting it with a certain noise. This models the fact that odometry measurements can be inaccurate due to, for example, slippage or uncalibrated parameters. Further details about odometry models can be found elsewhere [10,33].

With regard to the transition model of the beacons' offsets, our approach is backed-up by the following observation: the apparent offset of UWB ranges due to multipath typically remains constant until new obstacles enter or leave the LOS between the beacon and the mobile receiver. Since accurate models for these effects would be extremely hard to obtain, we propose the following approximate solution. At each time step, and for each beacon k, the random offset b_t^k does not suffer any change, that is, $b_t^{k,[i]} = b_{t-1}^{k,[i]}$ with a probability $1 - P_c$, where the probability of change is given by the parameter $P_c \in [0, 1]$, which depends on the structure of the environment. In case of changing an offset, its increment is modelled as a uniform distribution, with the constraint that the resulting value cannot be negative. The maximum value of this uniform distribution should be chosen accordingly to the specific scenario where the robot will operate. For example, in the experiments discussed later on we have set this limit to roughly the larger dimension of the scenario. In this way, if the sensed ranges become larger than this limit we will be sure than they are invalid measurements, and will have a negligible effect in the particle filter, since the mismatch will be roughly the same for all the particles.

At this point we have described the basis of particle filtering using the system transition model as the proposal distribution $q(\cdot)$. We must remark that this choice leads to a highly efficient implementation, although other proposal functions may be considered for a sufficiently large number of beacons. From our real experiments and simulations we have verified that our choice for the proposal distribution is well-suited to a practical number of UWB beacons, e.g. up to 10 beacons at sight at each instant of time.

We have also employed the optimal sampling approach described in [3] as an alternative to the above discussed method, and the results reveal a similar computational cost. Nevertheless, in the optimal sampling method the number of samples can be reduced by two or more orders of magnitude, hence it presents a clear advantage in memory storage (only a few particles must be kept). This advantage may become determinant as the number of beacons in a map grows. In this paper we do not further investigate this issue since in the experiments we deal with only three UWB beacons.

3.2. *Probabilistic Observation Model*

As it can be observed in Eq. (5), particle weights are updated through the observation likelihood function $p(z_t|s_t^{[i]})$. The intuitive idea behind this process is to assign high weights to those hypotheses that best explain the sensor readings, discarding in the resampling steps those particles that perform poorly. Without loss of generality we consider that the observation z_t contains simultaneous range readings for all the N beacon at each time step t. Formally, let the observation variable be the set:

$$z_t = \left\{z_t^1, ..., z_t^N\right\} \tag{6}$$

Since it is plausible to admit that the random errors in each of these individual measurements are independent, the observation likelihood can be factored as:

$$p\left(z_t|s_t\right) = \prod_{k=1}^{N} p\left(z_t^k|s_t\right) \tag{7}$$

Based on our experimental characterization, we model the range values as having an unknown offset b^k (which models the deviation of the measure due to multipath effects) plus a bias and an additive Gaussian noise characterized by $f(\cdot)$ and σ^2, respectively, as described in Eq. (1). Recall that $f(\cdot)$ models the sensor bias, that is, the systematic error that the UWB sensor always introduces in the sensed range, whereas the offset due to multipath, $b_t^{[i],k}$, must be estimated jointly to the robot pose. Then we can write down the desired likelihood function (for each

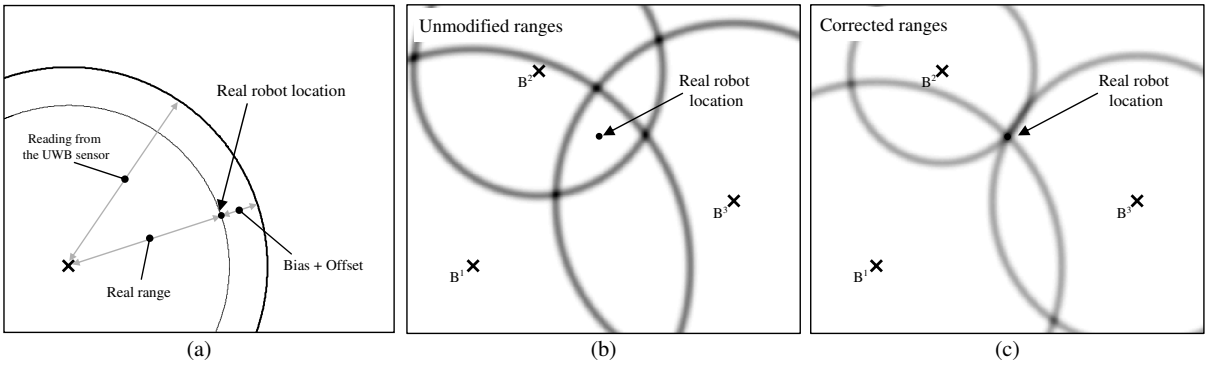

Fig. 9. (a) A schematic representation of the excess range measured by the UWB sensors: the measured range is comprised of the actual range between the antennas, plus the systematic error introduced by the sensors (bias) and the offset due to multipath. (b) An example of the joint observation likelihood for UWB range readings from three different beacons, where the excess range makes the real robot location to be assigned a negligible likelihood, whereas high values are assigned to wrong positions. (c) After correcting the ranges by subtracting the bias and the offset, we obtain a clearly defined maximum value of the likelihood at the right location.

range measurement z_t^k) as a Gaussian centered at the expected range, computed by adding the sensor bias $f(\cdot)$ and the particle's offset to the distance between the particle and the beacon, denoted by $r_t^{[i],k}$:

$$p\left(z_t^k | s_t^{[i]}\right) = \mathrm{N}(z_t^k; \underbrace{r_t^{[i],k} + f(r_t^{[i],k}) + b_t^{[i],k}}_{\text{Expected range}}, \sigma^2) \quad (8)$$

To illustrate the model underlying this expression, consider the schematic representation in Figure 9(a) where the range given by a UWB device is considered to be larger than the actual distance between the beacon and the robot. This excess of range is a result of two effects: (i) the systematic bias that the sensor always introduces, and (ii) offsets due to multipath. Note that the first effect will always occur, hence it is introduced in the likelihood expression above in a fixed form by mean of the corresponding function $f(\cdot)$. In contrast, the offset is unknown and hence the hypothesis kept by each particle ($b_t^{[i],k}$) is used to compensate this effect in the likelihood expression. We can visualize the effects of this range correction by evaluating the observation likelihood for a set of beacons, as shown in Figure 9(b). Observe how locations far from the actual robot pose are assigned the highest likelihood values, which means that the particle filter would diverge and lose track of the robot localization. In contrast, when the ranges are corrected as in Figure 9(c), the real location of the robot is assigned a maximum likelihood, hence the filter would converge towards the right robot position.

It is important to point out that, despite UWB ranges do not provide a direct observation of the robot heading, an estimate of the full robot pose is delivered by our filter thanks to the information provided by the odometry. Nevertheless, in the event that the robot was equipped with two or more UWB devices on-board, a straightforward extension to the particle filter discussed in this section would provide instantaneous observations of the robot heading, thus improving the filter estimates.

Finally, we must account for not all the measurements in Eq. (6) to be available simultaneously (as in the real experiments described later on). In these cases the likelihood for the absent readings can be set to any arbitrary constant value. Looking at the general Bayesian filter equations in Eq. (3) it is clear that any constant value, i.e. arbitrary but equal for all the particles, does not modify the estimated probability distribution.

4. Experimental Results

This section presents the results of two representative experiments in which the robot, endowed with a mobile UWB transceiver, estimates its pose within different environments using three fixed UWB beacons. The first experiment (Section 4.1) is aimed at proving the validity of our experimental characterization of UWB range measurements in LOS. The second experiment (Section 4.2) tests the suitability of our augmented-state approach to capture multipath and offset-affected readings during pose esti-

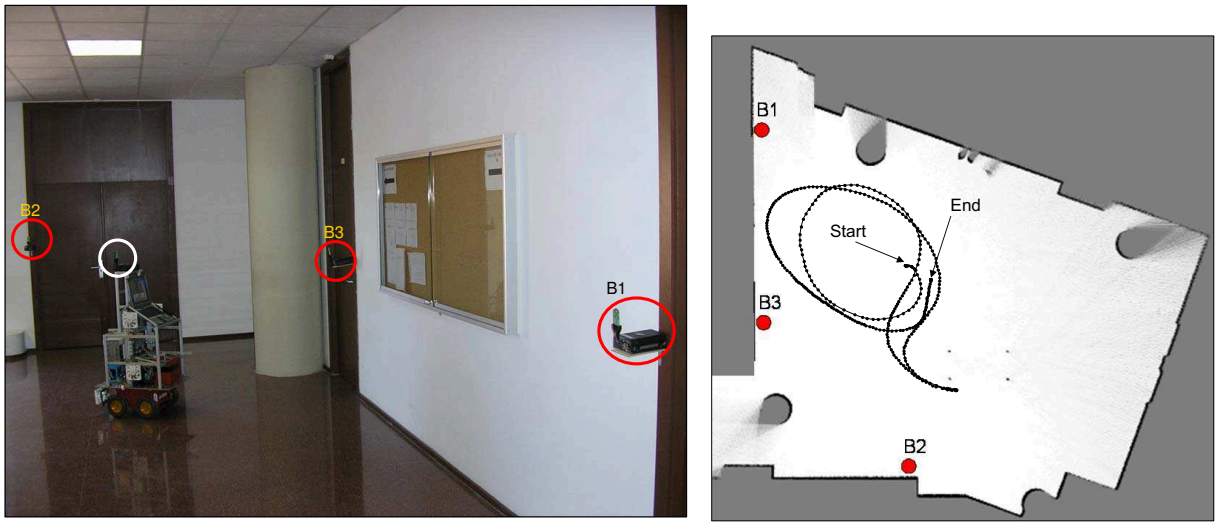

(a) (b)

Fig. 10. Mobile robot localization in a LOS environment. (a) The considered environment, an empty $13m \times 10m$ room that ensures the LOS between the antennas along the experiment. (b) Gridmap of the scenario, the position of the three UWB beacons and the ground-truth path followed by the robot.

mation [1]. It is important to remark that the scenarios chosen for these experiments are different to those considered in Section 2 for the sensor characterization.

4.1. *Robot Localization in LOS Environments*

Several experiments have been conducted in environments where the LOS between the robot onboard UWB device and the fixed beacons is assured at any time. We describe here the results of one of such experiments carried out within a $11.5m \times 10m$ empty room where three fixed UWB beacons were placed at known positions (see Figure 10). The mobile robot, equipped with a PulsOn UWB device [6] configured as "*master*" (receiver) and a laser scanner, is manually guided while recording UWB ranges, laser scans, and odometry information. These raw data are then processed offline for computing the robot pose. Although the proposed particle filter method is able to run in real time on a conventional computer [2], offline computation is adopted in this case for averaging different experiments (recall that PF is based on random sampling) and for comparing our approach to a pose-only state particle filter using exactly the same data.

The information from the laser scanner is used to compute a highly accurate estimation of the robot pose, which will be considered as the actual robot pose, i.e. the *ground-truth*. This is accomplished by matching scans against a map previously created also using the scanner laser. This scan matching method is based on an accurate ICP technique, whose results have a precision of roughly ± 2 cm and ± 1 degrees [26].

In this experiment the robot takes 90 seconds in a path of 30.7 meters. Figure 11 shows a comparison between the real path of the robot (ground-truth) and that estimated by two particle filters: one with our proposed augmented state and the other with a standard pose only-state. The sensor model in both cases is given by Eq. (8). Charts depict the average results of both implementations executed 250 times and considering 15000 particles.

As expected, in this scenario where multipath effects are not present, both particle filters yield similar results with position errors under 5cm. More precisely, the average error for the pose-only state approach is 4.66cm and for the augmented-state is 4.47cm. This provides us an experimental validation

[1] Related multimedia material and source code are available online at `http://babel.isa.uma.es/mrpt/uwbpf/`

[2] Each iteration with 15000 particles takes 0.1s in a Pentium Core2 Duo @2.2Ghz.

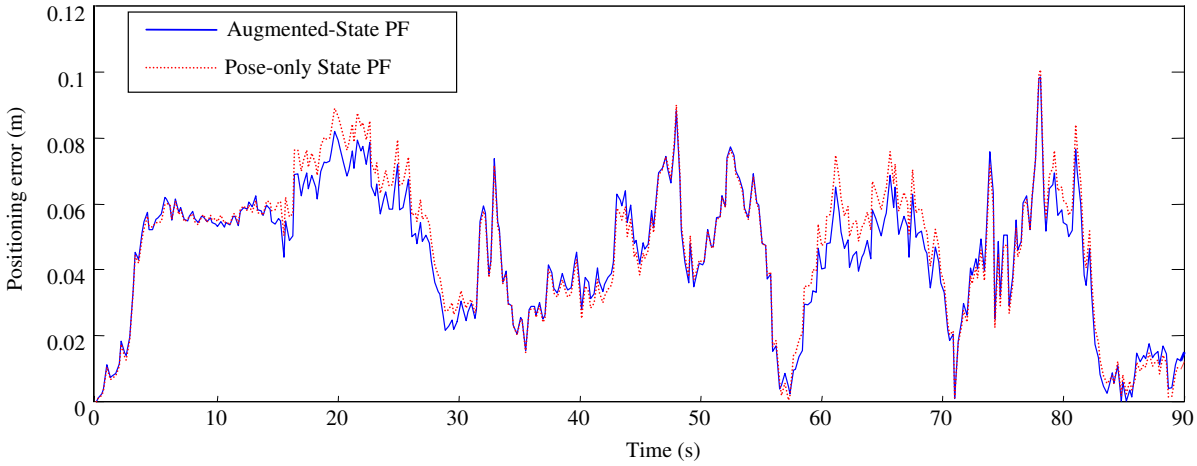

Fig. 11. Errors in the estimation of the robot path for both a pose-only state PF and our augmented-state approach. Notice that since there are no multipath effects, both errors are almost identical, and in average under 5 cm.

of the suitability of the proposed UWB range characterization for LOS configurations.

4.2. *Robot Localization under NLOS Conditions*

The aim of this second experiment is to test the suitability of our augmented-state PF (ASPF) approach for coping with multipath effects and the associated offsets in the measured ranges.

To this aim, we have conducted an experiment in a $12 \times 10m$ hall during 6 minutes approx. in which the robot is guided through an eight-shaped path of 108m (average speed of 0.3 m/s) around two metallic circular fences, as shown in Figure 13. Due to the particular characteristics of this environment and the location of the three beacons, multipath effects and temporary lost of signals occur at some specific spots, marked as A-F in Figure 13(b).

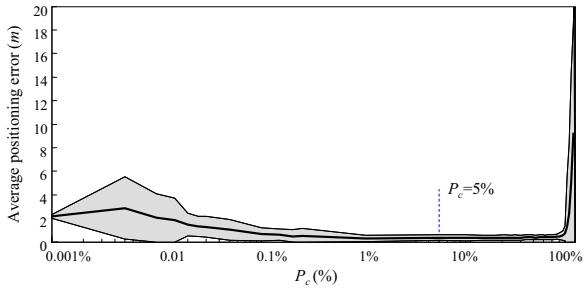

Fig. 12. The average positioning (x, y) error for different P_c parameter values. These results have been obtained executing our ASPF method 150 times for each P_c value. Confidence intervals of $\pm 2\sigma$ are represented by the shaded area.

As in the previous experiment, the ground-truth path was obtained from the laser scans and we have executed the two implementations of the PF, the pose only and the augmented-state versions, with 15000 particles each. For this sample population, the ASPF algorithm can perform in real-time since each iteration takes about 0.1s in a Pentium Core2 Duo @ 2.2Ghz. This roughly amounts to five times faster than real-time.

The probability of a beacon offset to change, P_c, is set to 0.05 in this experiment. This means that 1 out of 20 particles will change the offset of one beacon due to multipath at each time step. We have verified that, as long as the number of particles is large enough, such a value produces good results for a diversity of scenarios, though the method is not significantly sensitive to the chosen value of P_c. To prove this, we have computed the average positioning error of our ASPF method for different P_c values. The results, in Figure 12, reveal that for very low probabilities (notice that for $P_c = 0$ our method degenerates into the non-augmented PF) and for very high values (close to 1), the filter diverges giving overall errors of several meters.

Regarding the number of particles, it may seem that 15000 is an exceedingly large number of samples for performing pose tracking, as indeed is the case for more common robot localization using laser rangers [7]. The reason behind the need of such a large sample population in our approach is the "curse of dimensionality" which PFs suffer: in principle, the number of required samples increases exponentially with the number of dimensions in the problem. In

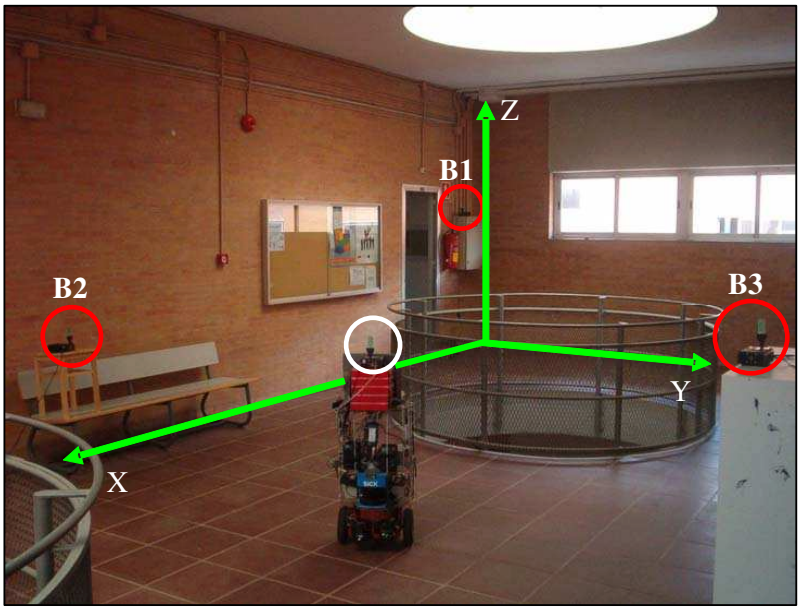

(a)

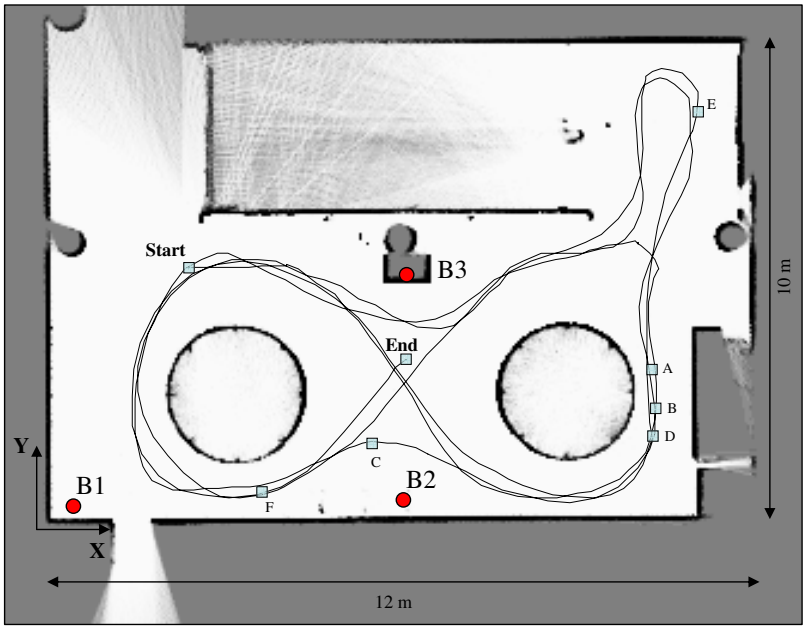

(b)

Fig. 13. Mobile robot navigating within an indoor environment at the corridors of the Computer Science building of the University of Malaga. (a) Picture of the environment where the positions of the UWB beacons as well as the coordinate system considered in this experiment are overprinted. (b) The position of the three UWB beacons and the ground-truth path followed by the robot, shown over a gridmap constructed from laser scans. Some interesting points are marked along the path as *A–F* for reference from the text.

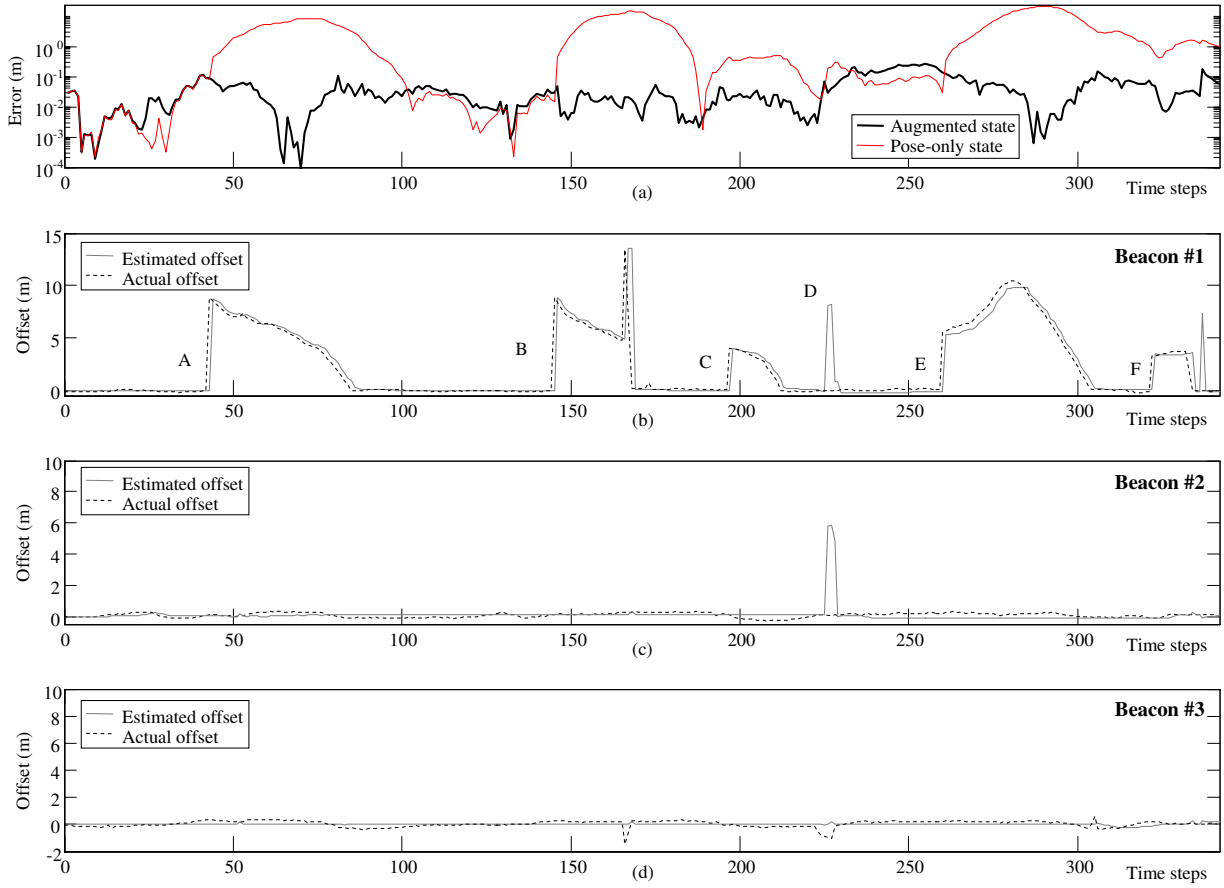

Fig. 14. (a) Positioning errors for both PF approaches. (b)–(d) The actual and the PF-estimated offsets in the beacon ranges. Refer to the text for further discussion.

this experiment, we have 6 dimensions, three for the robot pose plus one for each of the beacon's offset.

To illustrate the accuracy of our method, refer to Figure 14(a) where the positioning error is plotted for both PF methods. To understand this graph, we must also take into account the evolution of the real offsets of the beacons over time, represented in Figure 14(b)–(d) as dashed plots, which are computed from the sensor position on the robot and the ground truth path from laser scan matching. It is clear that the offsets estimated by our ASPF, the solid plots in those figures, closely follow the real offsets most of the time. This is the reason why our ASPF method drastically reduces the localization errors by more than one order of magnitude at those instants, as can be seen in Figure 14(a).

It is remarkable that most of the offset errors are contributed by beacon #1, and most of them occur at some specific spots of the environment, marked as A–F in the robot path. We must highlight an interesting behavior of our ASPF for the case denoted as D in Figure 14(b)–(d). In this case, the real offset change occurs in beacon #3, but due to the random nature of the transition model, the filter finds that a combination of offsets in beacons #1 and #2 also generates a situation compatible with observations. Although this leads to a slight (and temporary) increase in the positioning error, the filter quickly corrects itself. A solution to avoid events like this is to increase the number of samples.

An analysis of whether the ground-truth falls within the confidence interval given by the PFs provides us a good indication of their reliability. We show these confidence intervals separately for x, y and ϕ in Figure 15 for both PF methods. From the graphs it is clear that the error remains within a $\pm 3\sigma$ confidence interval most of the time for the ASPF, while in the pose-only PF errors often surpass several times this limit. Notice that the high orientation errors at the beginning of the experi-

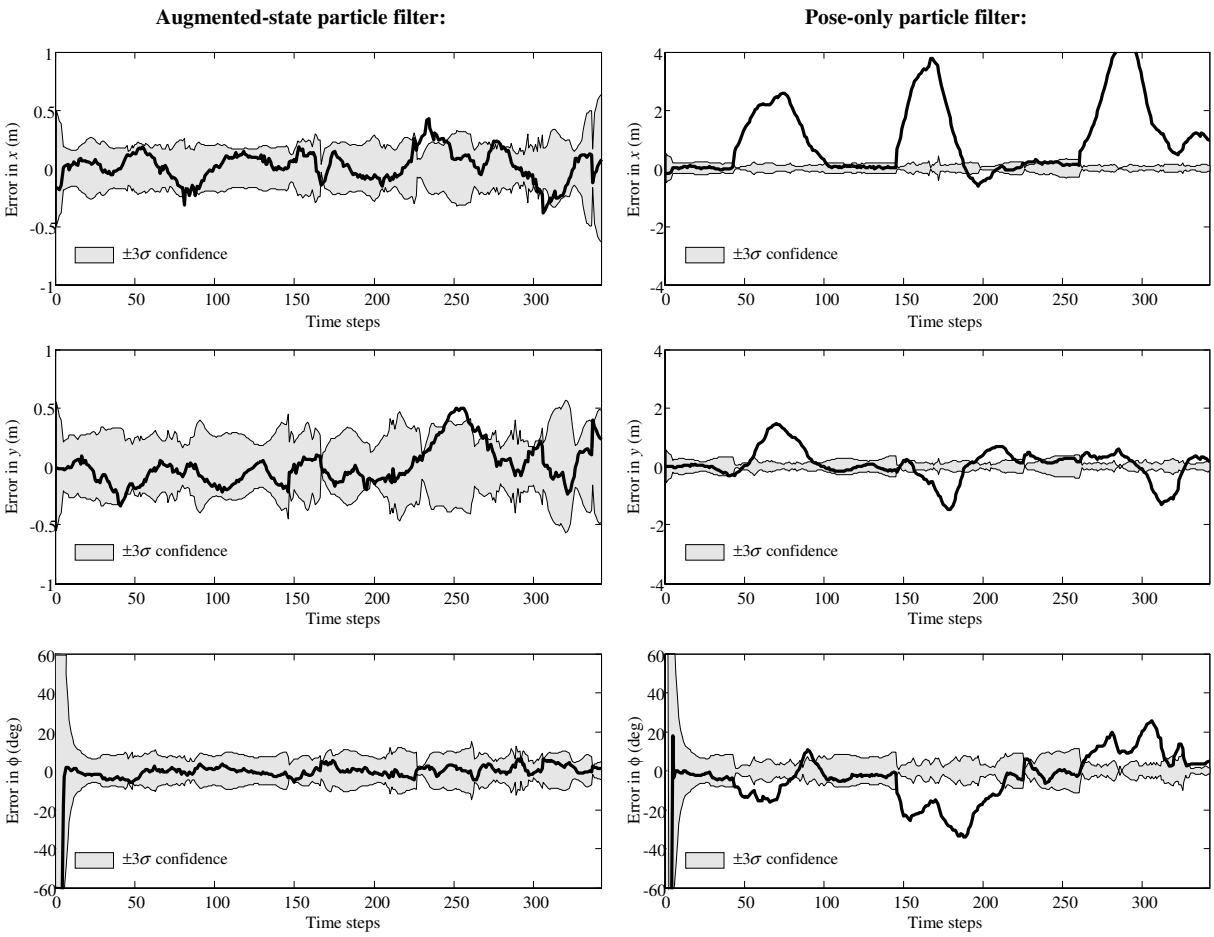

Fig. 15. The errors in positioning (x and y) and robot heading (ϕ) from both PF methods. We also represent the corresponding $\pm 3\sigma$ confidence intervals as shaded areas. It is clear that the augmented-state method discussed in this work outperforms the accuracy of the pose-only PF.

ment follows from the fact that no valid estimate of the heading can be obtained until the robot starts to move.

For the pose-only PF, the overall positioning errors (x, y) are of $1.75m$, while the mean heading error is $16deg$. For the ASPF, these errors reduce to $0.20m$ and $10deg$, respectively. Therefore, we can conclude that the ASPD correctly tracks the robot position *and* heading during most of the experiment with a relatively small error, in despite of having just incremental and inaccurate information from the vehicle's odometry. As previously commented, the heading estimate could be greatly improved by installing two UWB receivers on-board.

5. Conclusions and Future Work

This paper has approached the problem of robot positioning using UWB technology under the point of view of sequential Bayesian inference and in the form of particle filtering. An experimental characterization of UWB ranges has been presented within a variety of environments and situations, testing its suitability for estimating the pose of a mobile robot.

The proposed characterization covers both the cases in which UWB transceivers are in line of sight (no multipath effects are present) and those cases where multipath effects appear. To cope with multipath, a variation of the common PF approach for robot localization is adopted, which consists of augmenting the system vector with random variables that capture the unforeseen behavior of UWB ranges

when signals reflect. Several experiments have been conducted on real robotic platforms revealing the suitability of the proposed UWB range characterization and of the considered PF approach.

Our work requires further research to allow its practical integration into industrial environments, for example by enabling the automatic determination of the beacon locations, hence avoiding the laborious and error-prone process of surveying them manually.

Acknowledgments

We have to thank to Prof. Andrea Tonello from the University of Udine, and to Paolo De Stefanis and Franco Cattapan from Labor S.r.l., for their valuable comments and support during this work. The authors also thank Elena Cruz Martín for her valuable contributions to an early version of this paper.

This work has been supported by EU project CRAFT-COOPCT-2005-017668.

References

[1] B. Alavi, N. Alsindi, and K. Pahlavan. UWB Channel Measurements for Accurate Indoor Localization. *Military Communications Conference*, pages 1–7, 2006.

[2] B. Alavi and K. Pahlavan. Modeling of the distance error for indoor geolocation. *IEEE Wireless Communications and Networking*, 1, 2003.

[3] J.L. Blanco, J. Gonzalez, and J.A. Fernández-Madrigal. An optimal filtering algorithm for non-parametric observation models in robot localization. In *IEEE International Conference on Robotics and Automation (ICRA'08)*, pages 461–466, May 2008.

[4] J. Blumenthal, R. Grossmann, F. Golatowski, and D. Timmermann. Weighted centroid localization in Zigbee-based sensor networks. *Intelligent Signal Processing, 2007. WISP 2007. IEEE International Symposium on*, Oct. 2007.

[5] Federal Communications Commission. Broadband Internet Access Among Uses Envisioned by FCC Authorization of Ultra-Wideband Technology, 2002.

[6] TimeDomain Corporation. http://www.timedomain.com.

[7] F. Dellaert, D. Fox, W. Burgard, and S. Thrun. Monte Carlo localization for mobile robots. In *Proceedings of the IEEE International Conference on Robotics and Automation*, volume 2, 1999.

[8] B. Denis, J. Keignart, and N. Daniele. Impact of NLOS propagation upon ranging precision in UWB systems. *IEEE Conference on Ultra Wideband Systems and Technologies*, pages 379–383, 2003.

[9] A. Doucet, N. de Freitas, and N. Gordon. *Sequential Monte Carlo methods in practice*. Springer, 2001.

[10] A.I. Eliazar and R. Parr. Learning probabilistic motion models for mobile robots. *ACM International Conference Proceeding Series*, 2004.

[11] A. Eltaher and T. Kaiser. Positioning of Robots using Ultra-wideband Signals. *IRA workshop on Advanced control and Diagnosis*, 2004.

[12] R. Fleming, C. Kushner, G. Roberts, and U. Nandiwada. Rapid acquisition for ultra-wideband localizers. *IEEE Conference on Ultra Wideband Systems and Technologies*, pages 245–249, 2002.

[13] R.J. Fontana and S.J. Gunderson. Ultra-wideband precision asset location system. *IEEE Conf. on Ultra Wideband Systems and Technologies*, pages 147–150, 2002.

[14] A. Fort, C. Desset, J. Ryckaert, P. De Doncker, L. Van Biesen, and P. Wambacq. Characterization of the Ultra Wideband Body Area Propagation Channel. *IEEE International Conference on Ultra-Wideband*, pages 22–27, 2005.

[15] S. Geng, S. Ranvier, X. Zhao, J. Kivinen, and P. Vainikainen. Multipath Propagation Characterization of Ultra-wide Band Indoor Radio Channels. *IEEE International Conference on Ultra-Wideband*, pages 11–15, 2005.

[16] S. Gezici, Z. Tian, G.B. Giannakis, H. Kobayashi, A.F. Molisch, H.V. Poor, and Z. Sahinoglu. Localization via ultra-wideband radios: a look at positioning aspects for future sensor networks. *IEEE Signal Processing Magazine*, 22(4):70–84, 2005.

[17] Z. Irahhauten, GJM Janssen, and H. Nikookar. Characterization of the UWB Channel Based on Random Partially Known Frequency Responses. *IEEE International Conference on Ultra-Wideband*, pages 103–107, 2005.

[18] E. Jonietz. Ultra Wideband Wireless. *Magazine of Innovation Technology*, 2004.

[19] D.B. Jourdan, J.J Deyst Jr, M.Z. Win, and N. Roy. Monte Carlo Localization in Dense Multipath Environments Using UWB Ranging. *IEEE International Conference on Ultra-Wideband*, pages 314–319, 2005.

[20] S.J. Julier and J.K. Uhlmann. A new extension of the Kalman filter to nonlinear systems. *Int. Symp. Aerospace/Defense Sensing, Simul. and Controls*, 3, 1997.

[21] S.J. Julier, J.K. Uhlmann, and H.F. Durrant-Whyte. A new approach for filtering nonlinear systems. In *Proceedings of the American Control Conference*, volume 3, pages 1628–1632, 1995.

[22] R.E. Kalman. A new approach to linear filtering and prediction problems. *Journal of Basic Engineering*, 82(1):35–45, 1960.

[23] C.M. Keller and D.P. Young. Ultra-Wideband (UWB) Signal Localization Using a Vehicle-Sized Array. *IEEE International Conference on Ultra-Wideband*, pages 290–295, 2005.

[24] A. M. Ladd, E. K.E. Bekris, A.P. Rudys, D.S. Wallach, and L.E. Kavraki. On the feasibility of using wireless Ethernet for indoor localization. *IEEE Transactions on Robotics and Automation*, 20(3):555–559, 2004.

[25] J.S. Liu. Metropolized independent sampling with comparisons to rejection sampling and importance

sampling. *Statistics and Computing*, 6(2):113–119, 1996.

[26] J.L. Martínez, J. González, J. Morales, Mandow A., and García-Cerezo A. Genetic and ICP Laser Point Matching for 2D Mobile Robot Motion Estimation. *Journal of Field Robotics*, 23, January 2006.

[27] I. Oppermann, L. Stoica, A. Rabbachin, Z. Shelby, and J. Haapola. UWB wireless sensor networks: UWEN-a practical example. *IEEE Communications Magazine*, 42(12):S27–S32, 2004.

[28] B. Ristic, S. Arulampalam, and N. Gordon. *Beyond the Kalman Filter: Particle Filters for Tracking Applications*. Artech House, 2004.

[29] D.B Rubin. Using the SIR algorithm to simulate posterior distributions. *Bayesian Statistics*, 3:395–402, 1988.

[30] J. Schroeder, S. Galler, and K. Kyamakya. A Low-Cost Experimental Ultra-Wideband Positioning System. *IEEE International Conference on Ultra-Wideband*, pages 632–637, 2005.

[31] S. Shoval, I. Zeitoun, and E. Lenz. Implementation of a Kalman filter in positioning for autonomous vehicles, and its sensitivity to the process parameters. *The International Journal of Advanced Manufacturing Technology*, 13:738–746, 1997.

[32] B. Sohn, J. Lee, H. Chee, and W. Yu. Localization system for mobile robot using wireless communication with IR landmark. In *Proc. 1th International Conference on Robot Communication and Coordination*, Athens (Greece), 2007.

[33] S. Thrun, W. Burgard, and D. Fox. *Probabilistic Robotics*. The MIT Press, September 2005.

[34] A. Ward, A. Jones, and A. Hopper. A new location technique for the active office. *IEEE Personal Communications*, 4:42–47, 1997.

[35] MZ Win and RA Scholtz. Characterization of ultra-wide bandwidth wireless indoor channels: a communication-theoretic view. *IEEE Journal on Selected Areas in Communications*, 20(9):1613–1627, 2002.

[36] L. Yang and GB Giannakis. Ultra-wideband communications: an idea whose time has come. *IEEE Signal Processing Magazine*, 21(6):26–54, 2004.